J. Fluid Mech. (1988), *vol.* 197, *pp.* 571–594
Printed in Great Britain

Interaction of impulsively generated vortex pairs with bodies

By J. HOMA, M. LUCAS AND D. ROCKWELL
Department of Mechanical Engineering and Mechanics, Lehigh University, Bethlehem, PA 18015, USA

(Received 7 April 1987 and in revised form 3 May 1988)

A vortex pair, impulsively generated from a planar nozzle, is shown to have a degree of vorticity concentration in good agreement with inviscid theory, providing well-posed initial conditions for interaction with basic types of bodies (cylinders and plates). The scale of these bodies ranges from the same order as, to over an order of magnitude smaller than, the scale (distance between centres) of the incident vortex pair.

The fundamental case of a (primary) vortex pair symmetrically incident upon a very small cylinder shows rapid growth of a secondary vortex pair. These secondary vortices quickly attain a circulation of the same order as that of the corresponding primary vortices within a distance smaller than the lengthscale of the primary vortex pair. At this location, the temporal variation of integrated vorticity of primary and secondary vortices attains a maximum simultaneously. This zero phase shift between arrival of vorticity maxima provides the basis for formation of counter-rotating, primary–secondary vortex pairs, where both the primary and secondary vortices move at the same phase speed.

Visualization shows that the mode of secondary vortex formation is highly sensitive to the degree of symmetry of the initial encounter of the incident vortex pair with the body. The symmetrical mode of (in-phase) secondary vortex formation shows very rapid growth of large-scale secondary vortices; their development is relatively independent of the particulars of body shape and scale. On the other hand, the antisymmetrical mode takes two basic forms: large-scale secondary vortex formation, with the phase shift between their formation determined by the lengthscale of the body; and small-scale, antisymmetrical shedding of secondary vortices from the body occurring for a body lengthscale an order of magnitude smaller than that of the incident vortex pair. Correspondingly, there are several types of distortion of the cores and trajectories of the primary (incident) vortices.

1. Introduction

The interaction of unsteady vorticity fields with solid surfaces of varying scale and geometry is a problem of central importance in the area of aero/hydroacoustics, drag reduction, and heat transfer. Bushnell (1984) has recently addressed the wide range of investigations from relatively coherent concentrations of vorticity to fully 'turbulent' flows interacting with solid bodies. For the case of relatively coherent concentrations of vorticity in periodic flows, Rockwell (1983, 1984) reviews selected aspects of analytical and experimental advances in recent years. Characteristic of nearly all concentrated vorticity–surface interactions is generation of a secondary region of fluctuating vorticity. It may take on a distributed or

concentrated form, depending upon the precise details of the interaction mechanism. There have been a number of investigations of this type of interaction for flows along infinite and semi-infinite walls. In the following, we point out some of the observed mechanisms of the vortex–wall interactions.

Harvey & Perry (1971) first observed experimentally the process of unsteady separation and vortex formation arising from the interaction of a trailing vortex with the ground. Their total pressure surveys showed clearly that the primary (trailing) vortex induced a secondary vortex. A class of vortex–surface interactions that has received considerable attention recently involves the case of an axisymmetric ('ring') vortex incident upon a flat plate oriented normal to the axis of the vortex: Magarvey & MacLatchy (1964), Schneider (1978, 1980), Cerra & Smith (1983), Ho (1983) and Didden & Ho (1985). Cerra & Smith (1983) visualized various features of the interaction region. In the case of sufficiently strong primary vortices incident upon the plate, there arise not only secondary, but also tertiary vortex rings. The Biot–Savart interaction between these two types of vortex rings and the primary vortex ring as well produce a number of interesting interaction patterns. Didden & Ho (1985) focussed on a two-dimensional (axisymmetric) interaction and carried out detailed measurements of the fluctuating vorticity field in the primary vortex–plate interaction region; emphasis was on the process of flow separation leading to secondary vortex formation. They hypothesized that once the flow separated from the surface, the growth of the secondary vortex may be dominated by inviscid mechanisms. Such an interpretation is reinforced by the observations of Homa & Rockwell (1983) showing rapid growth of secondary vortices.

Still another class of flows involves generation of concentrated regions of secondary vorticity due to unstable, distributed (primary) vorticity incident upon a leading edge. Kaykayoglu & Rockwell (1985) have demonstrated that an oscillating planar jet, upon interaction with a leading edge, shows rapid evolution of a primary vortex arising from jet shear-layer instability and subsequent flow separation from the surface of the edge leading to secondary vortex formation. In turn, these vortices form a primary–secondary vortex pair that either erupts away from, or propagates downstream along, the edge. In the case of a row of periodic concentrations of vorticity upon a leading edge, Ziada & Rockwell (1982) and Kaykayoglu & Rockwell (1986) show that there is pronounced secondary vortex formation at the tip of the edge; it is due to sweeping of flow from the top to the bottom surface of the flow, a mechanism driven by the primary vortex–edge interaction. Theoretical simulation of this class of problems has ben carried out by Panaras (1985, 1986, 1987) using an inviscid discrete-vortex method. Although the process of secondary vortex generation is not encompassed in this approach, certain features of the primary vortex–surface interaction are well approximated.

The onset of flow separation due to primary vortex/boundary layer interaction has been analysed by Walker (1978) for the case of a line vortex passing above a flat plate of infinite extent; the calculations reveal that the boundary layer undergoes rapid thickening leading to formation of a secondary recirculation zone. Subsequently, Doligalski, Smith & Walker (1979) and Doligalski & Walker (1984) addressed further features of vortex–surface interactions such as the sign and convective speed of the primary line vortex as it travelled along the surface of the plate. In these studies, the mean velocity profile was of the boundary-layer type, in contrast to the wall-jet profiles associated with nearly all of the foregoing investigations.

Finally, we should note that there may be some parallels between the vortex–body

interactions addressed herein and the collision of a vortex pair with a row of mixing-layer vortices (Kiya, Ohyama & Hunt 1986).

To date, there has been no investigation of the interaction of concentrations of vorticity with bodies having finite streamwise length in absence of mean flow. In this study, we address the case where the scale of the incident vortex pair (distance between centres of vortices) ranges from the same order as, to two orders of magnitude smaller than, the characteristic dimension of the body.

2. Experimental system and instrumentation

An overview of the experimental arrangement, including the vortex generation system and the housing for support of the body, is given in figure 1. The vortex pair was generated by impulsive motion of a piston in a rectangular cross-section nozzle. The piston was driven by releasing a swinging arm and allowing it to fall freely to the terminal piston position. This swinging arm was raised by a computer-controlled motor–pully system which was synchronized with the laser-Doppler system described subsequently. Using this technique, it was possible to generate remarkably consistent vortex pairs, satisfying the condition that the rotational flow supplied by the piston motion must fill the entire cell of a vortex in a planar vortex pair. This structure of the planar vortex pair differs from that of its axisymmetric counterpart, for which the vorticity may occupy only a small cross-sectional toroid allowing, in some cases, vortex generation from small perturbations superimposed on a mean flow (Didden & Ho 1985).

Representative dimensions of the tank–nozzle system were as follows. The tank was 30.5 cm wide and 61 cm deep, and the nozzle width (w) and breadth (b) were 1.2 cm and 30.5 cm respectively. The length of the nozzle from the terminal position of the piston to the nozzle exit was 24.5 nozzle widths, i.e. $24.5w$. The distance from the initial to the terminal location of the piston, i.e. the piston stroke, was $15w$. The measured displacement of the piston as a function of time, $x(t)$, showed a rapid acceleration to an essentially uniform velocity. The total time required for the piston to travel the distance of its stroke was 1.6 s. Of this time 0.1 s was required for acceleration to a constant piston velocity, leaving 1.5 s at constant velocity. The constant velocity of the vortex pair was $U_c = 1.8$ cm/s and the distance between centres of the fully formed vortex pair was 2.0 cm. The corresponding Reynolds number based on nozzle width $w = 1.2$ cm was $Re = U_c w/\nu = 247$. The circulation of the fully formed vortex pair was determined from considering the line integral about a defined contour within the flow field, taking advantage of the fact that the velocity is essentially zero at locations well away from the measuring volume:

$$\Gamma = U_c \int_{-\infty}^{\infty} [U(t) - U_c]\,\mathrm{d}t,$$

wherein $U(t)$ and U_c were measured on the longitudinal centreline of the vortex pair with the laser system. Such a measurement is Eulerian; if it is assumed that the structure and convective speed of the (an impinging) vortex do not change over the streamwise lengthscale of the vortex pair, then determination of the velocity with time at a single point is appropriate. Velocity measurements were not made at locations well away from where the values of U_c and $U(t)$ were determined. However, since the distance from the vortex centreline to the other portions of the integration circuit were much larger than the scale D of the vortex pair, induced velocities there

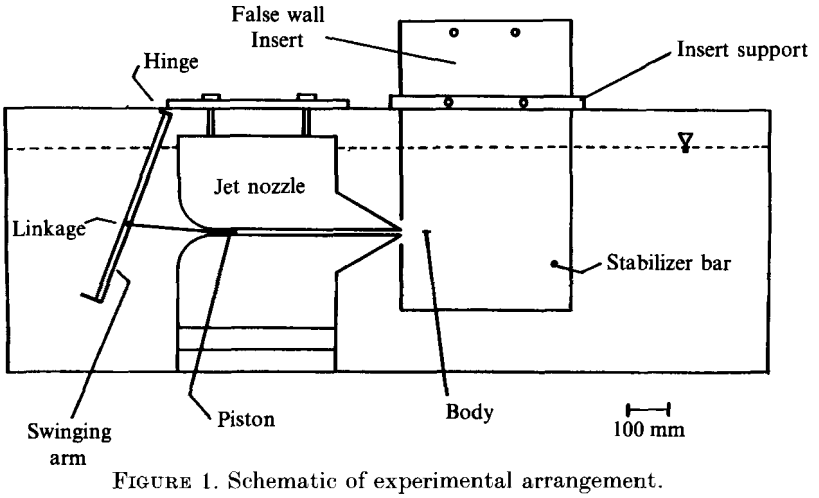

FIGURE 1. Schematic of experimental arrangement.

were negligible. This technique gave $\Gamma/U_c D = 5.5$, where D is distance between vortex centres. Laser measurements of the vorticity field and corresponding visualization described in this work were performed at $Re = 247$. During a visualization study of the effect of cylinder offset on vortex pair–cylinder interaction, a lower value of Reynolds number was employed, $Re = 165$. The basic features of the vortex structure and the interaction patterns were the same for these two values of Reynolds number. Extensive measurements of the trajectories of the generated vortex pairs, in conjunction with spanwise visualization, were made at off-centreline locations of the flow system to determine the precise extent of the two-dimensionality. For the flow domains of interest herein, the vortex patterns were essentially the same over 85% of the span. The character of the spanwise instability downstream of the regions investigated here was not determined.

Of primary interest in this investigation is the interaction of the generated vortex pairs with cylindrical- and plate-shaped bodies. The cylinders had diameters of 0.158 cm (brass) and 0.026 cm (highly taut fishing line) and the plates (brass) all had a thickness of 0.158 cm (with streamlined edges). All cylinders and plates were equipped with a 1.6 cm diameter pin protruding from both ends, allowing the plate or cylinder to be fitted into 6.4 mm thick (false) endwalls (see figure 1). The entire cylinder/plate endwall assembly could be lowered into the channel to the desired depth. The centre of each cylinder/plate was always located a distance of 6.25 cm from the nozzle exit.

Time-dependent measurements of the longitudinal and transverse velocity components, $u(t)$ and $v(t)$, were made with a laser-Doppler system employing a 2 W Argon-ion laser operating in the backscatter mode. By using a beam expander, it was possible to enhance the signal-to-noise ratio by a factor of approximately 50. Silicon carbide particles were used to provide uniform scattering, thereby giving a high data rate and allowing use of the analog output of the counter which was, in turn, linked to the MINC minicomputer. The time interval of data sampling was $\Delta t = 0.005$ s. Since the vortex generation process was repeatable, it was possible to measure the u- and v-components independently and relate their phases to the trigger signal of the free-falling arm. By use of such a phase reference, all essential information for constructing the instantaneous vorticity $\omega(y, t)$ was generated. Further details of this technique are addressed in the next section.

Flow visualization involved a dye (blue food colouring) technique, whereby the dye was carefully laid upon the upper portion of the lower nozzle lip and the upper portion of the upper nozzle lip prior to release of the free-falling arm. Dye was injected from a hypodermic syringe through a $\frac{1}{8}$ in. tygon tube connected to a $\frac{1}{8}$ in. brass tube terminated by a $\frac{1}{32}$ in. tube. By allowing the dye on the upper lip to drip downwards across the nozzle exit prior to the onset of piston motion, one obtains a timeline marker which indicates the front portion of the vortex. This marker is evident in nearly all the visualization photos shown herein. Moreover, after the onset of a piston motion, the dye on the nozzle lips marks the locus of shed vorticity, forming a corresponding streakline pattern.

Films of the visualized vortex, which were correlated with the instantaneous vorticity, were made with an Instar video system, which had a framing rate of 120 frames/s. Selected visualization films were synchronized with the laser velocity measurements using the audio channel on the video system as a phase reference.

3. The structure of the incident vortex

The nature of the incident vortex–body interaction is not simply a function of the circulation of the incident vortex, but the degree of concentration of vorticity with respect to the lengthscale of the body. In determining the vorticity distribution $\omega(y)$ across the incident vortex, measurements of the instantaneous longitudinal and transverse velocity components, $u(t)$ and $v(t)$, were taken at the measurement station $x/D = 1.8$, where x is distance downstream of the nozzle exit and D is distance between vortex centres of the formed pair. These data were acquired at ten values of time t, using the initiation of piston motion as a zero time reference. By correlating these times with dye visualization of the vortex on the high-speed video system, it was possible to determine the instantaneous vorticity $\omega(y, t)$ at successive stages of the visualized vortex–cylinder interaction in relation to the visualized vortex.

In theoretically describing the structure of the incident vortex for comparison with the vorticity measurements, it is possible to assume two extreme distributions of vorticity: concentrated in two line vortices symmetrically located about the centreline of the vortex pair; or, distributed throughout each vortex. For the case of line vortices, originally analysed by Lamb (1932), the recirculation cell of the vortex takes the shape of an oval that encloses both vortices; the resultant motion is steady. It is possible, however, to retain the conditions for the steady motion of the vortex pair in the case where the vorticity is distributed throughout the recirculation cell assuming that the relation

$$\omega = k^2\psi$$

is valid throughout the domain of non-zero vorticity (Batchelor 1967). The governing equation in terms of stream function ψ and constant k takes the form

$$\frac{\partial^2\psi}{\partial r^2} + \frac{1}{r}\frac{\partial\psi}{\partial r} + \frac{1}{r^2}\frac{\partial\psi}{\partial\theta^2} = -k^2\psi.$$

Since it is desirable to match the vorticity-containing region with the external irrotational flow, one may take the irrotational domain as the flow past a circular cylinder, which suggests that $\psi \propto \sin\theta$. For this form of ψ, the solution is a Bessel function of the first order:

$$\psi = CJ_1(kr)\sin\theta.$$

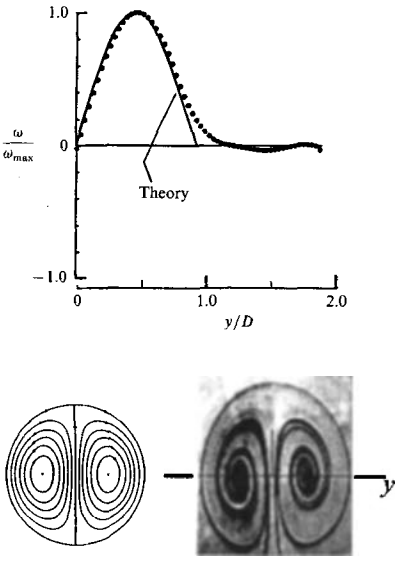

FIGURE 2. Structure of incident vortex pair in the forms of: visualization by streaklines emanating from lips of nozzle exit; theoretically determined streamline pattern; and comparison of experimental and theoretical (Batchelor 1967) distributions of vorticity across one-half of a vortex pair at an instant when the centres of vortices are coincident with the measuring station.

In this solution the circle $r = R$ bounds the recirculation cell; outside it the flow field is the same as that for irrotational flow past a circular cylinder of radius R in a uniform stream. We note that the distribution of vorticity in a typical vortex ring and the planar vortex pair of the kind described here are quite different. In the former, the recirculation cell takes the form of a toroid enclosing a well-defined irrotational region, whereas for the planar vortex pair it is in the form of an oval (Lamb 1932) or circle (Batchelor 1967) that encloses both vortices.

In figure 2, we compare the visualized streakline pattern and the theoretically calculated streamlines (Batchelor 1967, p. 535) of the vortex pair with the experimentally determined distribution of vorticity at a time when its centres are at the vorticity measuring station. The theory (Batchelor 1987) is indicated by the solid line. Theoretical and experimental vorticity distributions have been normalized with respect to their peak amplitudes. It is evident that the vorticity is highly distributed and there is good agreement of the shape of $\omega(y)$ with theory. We note that even though the Reynolds number $Re = U_c D/\nu = 247$ is relatively low, the inviscid theory is adequate.

4. The structure of the basic vortex pair–body interaction

Interaction of the vortex pair defined in figure 2 with a body will give rise to secondary vortices downstream of the body, e.g. see photos of figure 7. Consequently, it is necessary to characterize the primary–secondary vorticity field in this region. Since we are examining non-sinuosidal, transient variations of vorticity, it is necessary to follow the entire variations of $u(t)$ and $v(t)$ rather than simply determining their amplitudes and phases with respect to a sinusoidal reference. Data acquisition is, therefore, a voluminous undertaking and it was decided to focus on the most representative cross-section of the flow, within constraints imposed by the

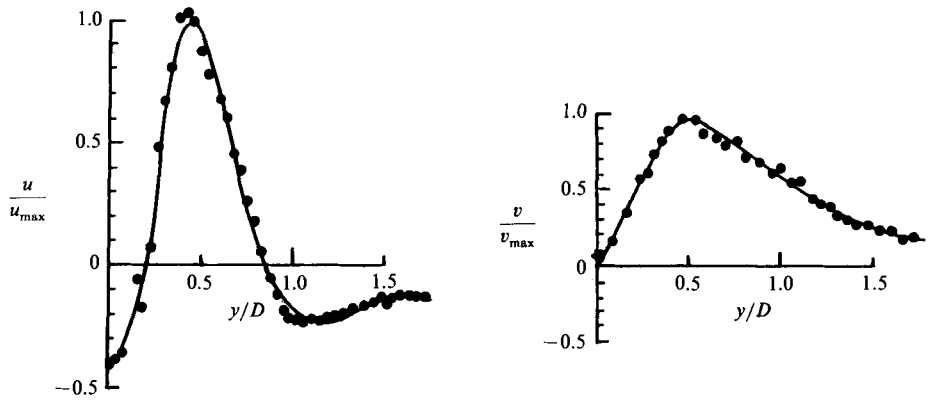

FIGURE 3. Typical distributions of longitudinal (u) and transverse (v) velocity fluctuations at representative section $x/D = 0.45$ where formation of the secondary vortex is clearly evident; $x \equiv$ distance downstream of cylinder, $D \equiv$ distance between centres of incident vortex pair. Data taken at instant when centres of primary vortices are coincident with the measuring station. Solid line represents computer-generated curve fit.

optical arrangement of the LDA. After consideration of flow visualization and preliminary measurements of a symmetrical vortex–cylinder interaction which clearly exhibited the principal features of the secondary vortex formation, a cross-section at $x/D = 8(x/D = 0.45)$ was selected. Coordinate x is measured from the centre of the cylinder. At this section the secondary vorticity fluctuations have experienced considerable growth in the region immediately behind the cylinder, and the primary vorticity field has undergone the initial stage of distortion and movement away from the centreline.

The distributions of longitudinal and streamwise velocity components u and v were acquired using the piston motion as a phase reference, in the same fashion as in the foregoing characterization of the approach vortex. A total of fifty-one measurement locations were considered across the flow. Figure 3 shows typical curve fits to the instantaneous data taken when the centre of the dye concentration of the primary vortex is coincident with the measuring volume. From such curve fits, one may construct a family of curves for the u- and v-components spanning a range of time before and after the passage of the primary vortex. Such a family is shown for the u-component in figure 4. It is evident that the maximum negative and positive values of u occur when the centre of the primary vortex pair is coincident with the measuring station. These maxima are attained at $t^* \equiv U_c t/D \approx 2.5$, corresponding to the extremum of the distributed vorticity of the primary vortex, addressed below in conjunction with figure 5.

Using these instantaneous curves in conjunction with a similar family for the v-component, it is possible to construct contours of constant vorticity $\omega(x, t)$ on the (y, t)-plane, as shown in figure 5. In constructing these contours, a total of 101 time stations were considered, corresponding to 100 slices on the $U_c t/D$ axis of figure 5. In evaluating the $\partial v/\partial x$, three streamwise stations (spaced by 2.5 mm) were considered, the central one corresponding to the measurement station of u; the values of $\partial v/\partial x$ then followed from evaluation of a central-difference method. The upper set of vorticity contours corresponds to the primary vortex, and the lower set to the secondary vortex, both located above the centreline of the flow field. Regarding the primary vortex, its centre is essentially coincident with the

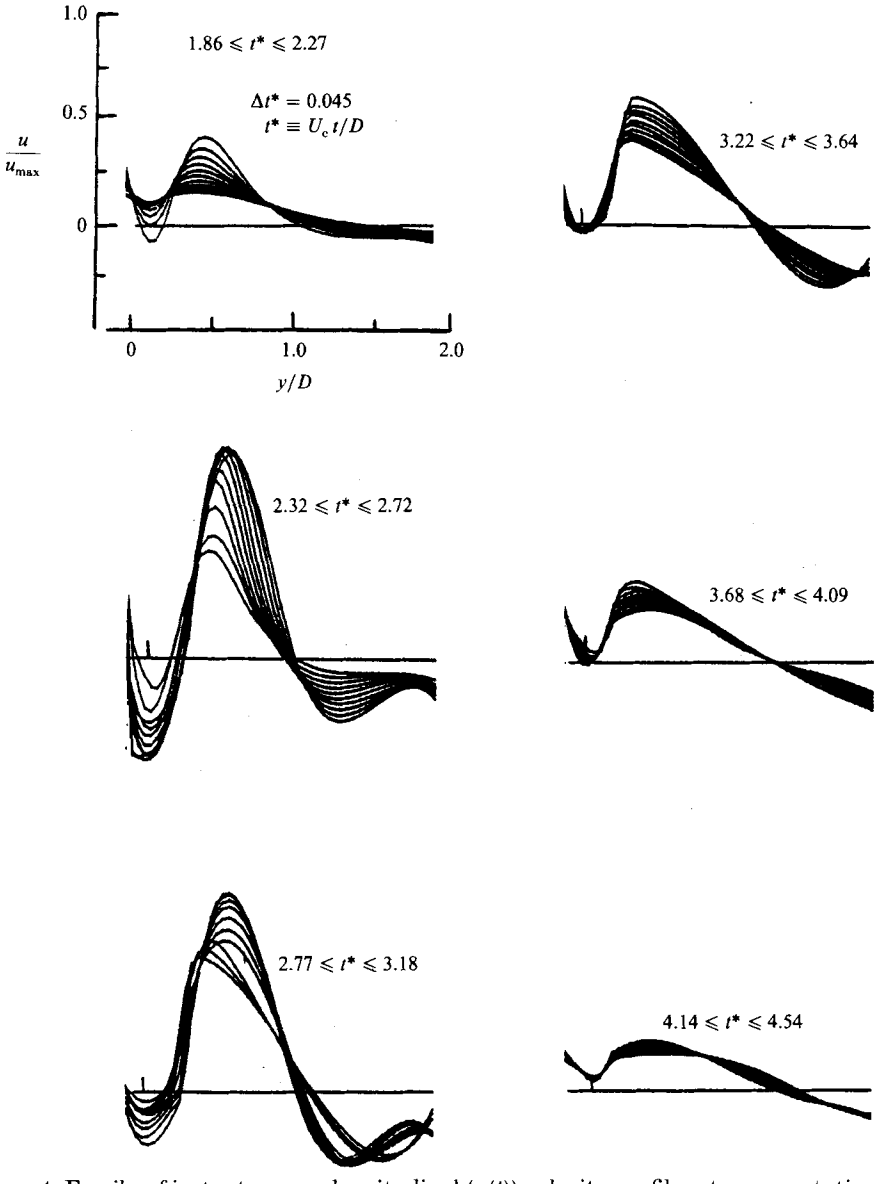

FIGURE 4. Family of instantaneous, longitudinal ($u(t)$) velocity profiles at representative section $x/D = 0.45$; $x \equiv$ distance downstream of cylinder, $D \equiv$ distance between centres of incident vortex pair. Range of time corresponds to incident vortex pair upstream of, at, and downstream of measuring station.

corresponding centre of the dye concentration in figure 5, within the experimental uncertainty of the correlation between video visualization and vorticity measurements. Moreover, the secondary vortex rollup shown in the photos of figure 5 corresponds to an elongated concentration of vorticity whose tail extends to large time, indicating that vorticity is continuously shed from the cylinder well after passage of the primary vortex. The front of the region of secondary vorticity has a vorticity gradient somewhat steeper than the primary vortex, and its vorticity maximum occurs slightly earlier than the primary vortex, i.e. compare contour lines over $1.75 \leqslant U_c t/D \leqslant 2.5$.

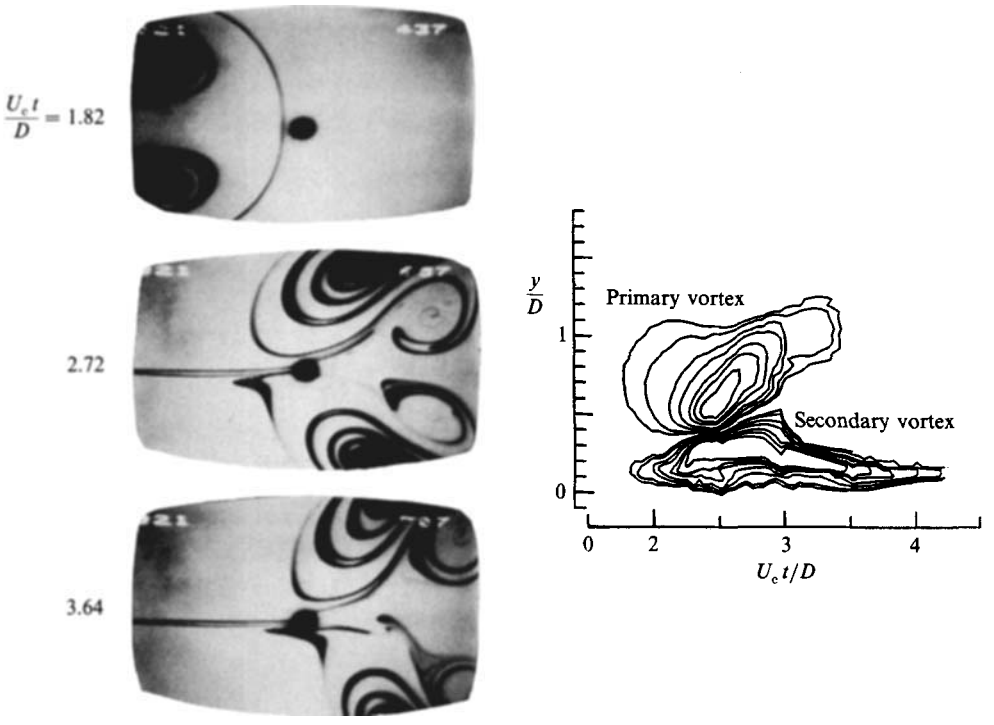

FIGURE 5. Photos showing sequence of vortex pair–cylinder interaction and contours of constant vorticity taken at representative section $x/D = 0.45$; $x \equiv$ distance downstream of cylinder; $D \equiv$ distance between centres of incident vortex pair depicting primary vortex (upper set of contours) and secondary vortex (lower set of contours). In each contour set, the outermost contour represents $\omega = \pm 0.05$; the difference between contours is $\Delta\omega = 0.05$.

Employing the transformation $x = U_c t$ and spatially integrating the vorticity to determine the circulation of the primary and secondary vortices respectively, the circulation ratio of the secondary to primary vortex is $\Gamma_{sv}/\Gamma_{pv} = -1.18$. In carrying out this integration, elemental spatial domains of area $\Delta X \Delta Y = 0.85 \times 10^{-3}$ cm^2 were employed. With respect to the scale of the incident vortex pair, this corresponds to $D^2/\Delta x \Delta y = 583$. Of course, downstream of the measuring station ($x/D = 0.45$) shown in figure 5, there is still some distortion of the vorticity field, and there is a degree of inaccuracy involving the transformation $x = U_c t$. Such a transformation is commonly employed, for example, in describing developed vortices translating in free space (Sullivan, Widnall & Ezekiel 1973).

As another indication of growth of the secondary vortex immediately behind the cylinder, one may examine the temporal variation of an integral of the vorticity for both the primary and secondary vortices at the same value of parameters and measuring station as for figure 5. We define a parameter $W(t)$ as

$$W(t) \equiv \int \omega^2(y, t)\, \mathrm{d}y.$$

It has been evaluated independently for the regions of primary and secondary vorticity. From the plot of figure 6, it is evident that convection of the fronts of both the primary and secondary vortices (through the fixed plane at $x/D = 0.45$) yields an exponential growth in vorticity exponential growth in vorticity amplitude $W(t)$. The

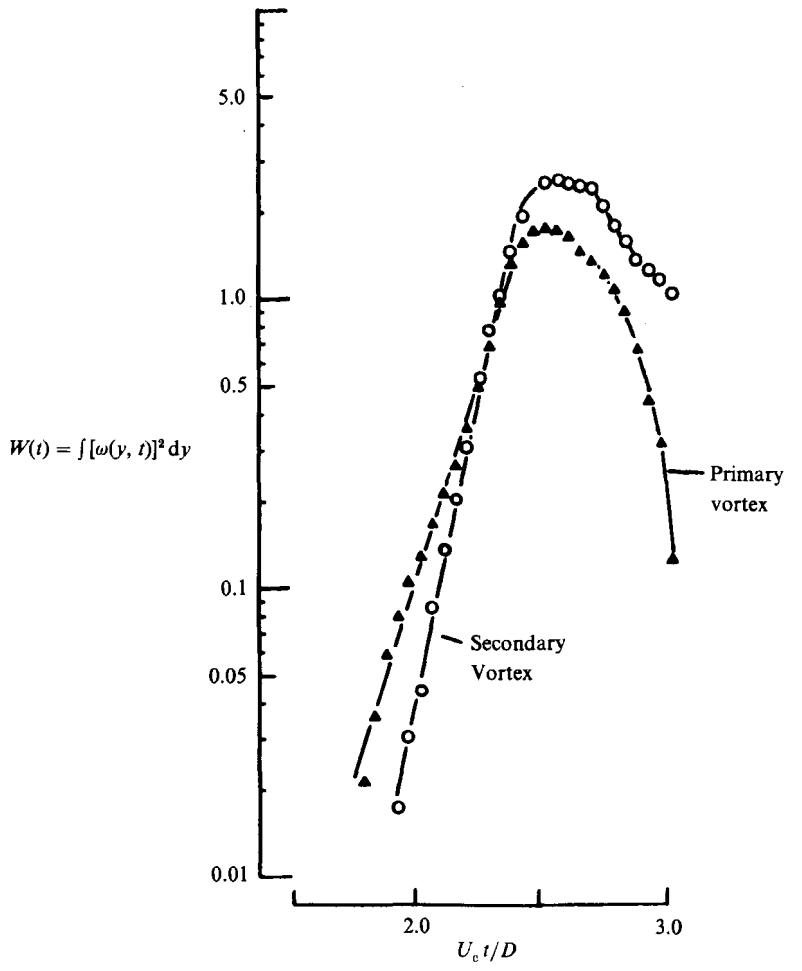

FIGURE 6. Variation of parameter $W(t)$ for both the primary and secondary vortices with time at station $x/D = 0.45$; $x \equiv$ distance downstream of cylinder and $D \equiv$ distance between centres of incident vortex pair.

rate of growth of the secondary vortex somewhat exceeds that of the primary vortex. Both vortices attain maximum $W(t)$ at the same value of time, i.e. $U_c t/D = 2.5$; in other words, there is essentially zero phase shift between the vorticity maxima W of the primary and secondary vortices. It is this zero shift that promotes formation of the primary–secondary vortex pair, evident at larger $U_c t/D$ in figure 5. Upstream of this region, flow separation from the cylinder, leading to secondary vortex formation, is induced by the primary vortex having a given spatial distribution of vorticity; we expect that there is a small phase shift between the arrival of the vorticity maximum of the primary vortex and the onset of flow separation, in turn allowing establishment of the zero shift between maximum W of the primary and secondary vortices in the region immediately downstream of separation.

Concerning the decrease in $W(t)$ at larger values of time, $W(t)$ of the primary vortex rapidly drops off, in contrast to that of the secondary vortex, which shows a relatively slow, exponential decrease at large $U_c t/D$. This trend is due to the continued shedding of secondary vorticity after passage of the primary vortex, already evident in the tail of the vorticity contour plot of figure 5.

5. The structure of the vortex–cylinder interaction

In the foregoing, we have seen that symmetrical interaction of an incident vortex pair with a small cylinder gives rise to large-scale, symmetrical secondary vortex formation. In the event that the interaction process is not symmetrical, the issue arises as to whether large-scale secondary vortex formation is still possible. We expect the details of the interaction pattern to be a strong function of location of the cylinder with respect to the centre of the core of the primary vortex. In fact, as will be shown, a small departure from symmetry of the incident vortex pair with respect to the body causes an abrupt change to an antisymmetrical mode, characterized by small-scale vortex shedding from the cylinder, which can strongly affect the structure of the primary vortex. In the following, we classify the interaction patterns and modes of secondary vortex formation according to: the location of the centreline of the body with respect to the vorticity minimum of the incident vortices, i.e. equidistant between centres of the vortex pair; and vorticity maximum, i.e. at the vortex centre. Attention is focused on cylinders having a lengthscale at least an order of magnitude smaller than the lengthscale (distance between centres) of the incident vortex pair, thereby minimizing after-body effects in development of the secondary vortices from the cylinder.

Figure 7 shows the symmetrical mode of secondary vortex formation from the cylinder located equidistant between centres of the primary vortex pair. This interaction represents a complete sequence of the mechanism discussed in conjunction with figure 5. The first photo of figure 7 depicts the dye concentrations marking vortices A and B immediately before their encounter with the cylinder; the circular-shaped dye line ahead of the vortex pair was originally a vertical line of dye across the nozzle exit prior to the release of the piston, and therefore represents a timeline marker. This line shows, in successive photos, the initial process of secondary vortex formation. In the third to fifth photos, one sees that the secondary vortices C and D have grown to the extent that they draw the dye streaklines of the original primary vortex pair in the direction of secondary vortex rollup. The end result of this secondary vortex formation and distortion of the primary vortices are the primary–secondary vortex pairs AC and BD. At a distance of approximately $0.5D$ downstream of the cylinder, the trajectory of these newly formed vortex pairs is already at 45° with respect to the centreline of the flow field.

For this symmetrical shedding of secondary vortices, the question arises as to how small the cylinder can be, relative to the scale of the incident vortex pair, and still produce a substantial alteration of the trajectories of the primary vortices. Not shown here is the interaction with a cylinder (a 0.5 mm fishing line stretched taut across the test section) having a diameter a factor of six smaller than in figure 7, i.e. $d/D = 0.01$ (Homa 1984). In comparison with figure 7, the secondary vortices mature less rapidly; nevertheless, their presence can effect the distortion of the primary vortices as is evident in the later stages of the interaction. The trajectories of the primary vortices move outward significantly, as in figure 7.

Figure 8 shows antisymmetrical shedding of secondary vortices from the cylinder located between the centreline of the primary vortex pair and the centre of the primary vortex. This abrupt change from the symmetrical interaction described in the foregoing is induced by locating the cylinder slightly off centreline, $\epsilon/D = 0.12$. The mechanism of development of the secondary vortices is fundamentally different than that of the symmetrical vortex pair–cylinder interaction shown in figure 7. Whereas the symmetrical mode interaction described in figure 7 gave rise to large-

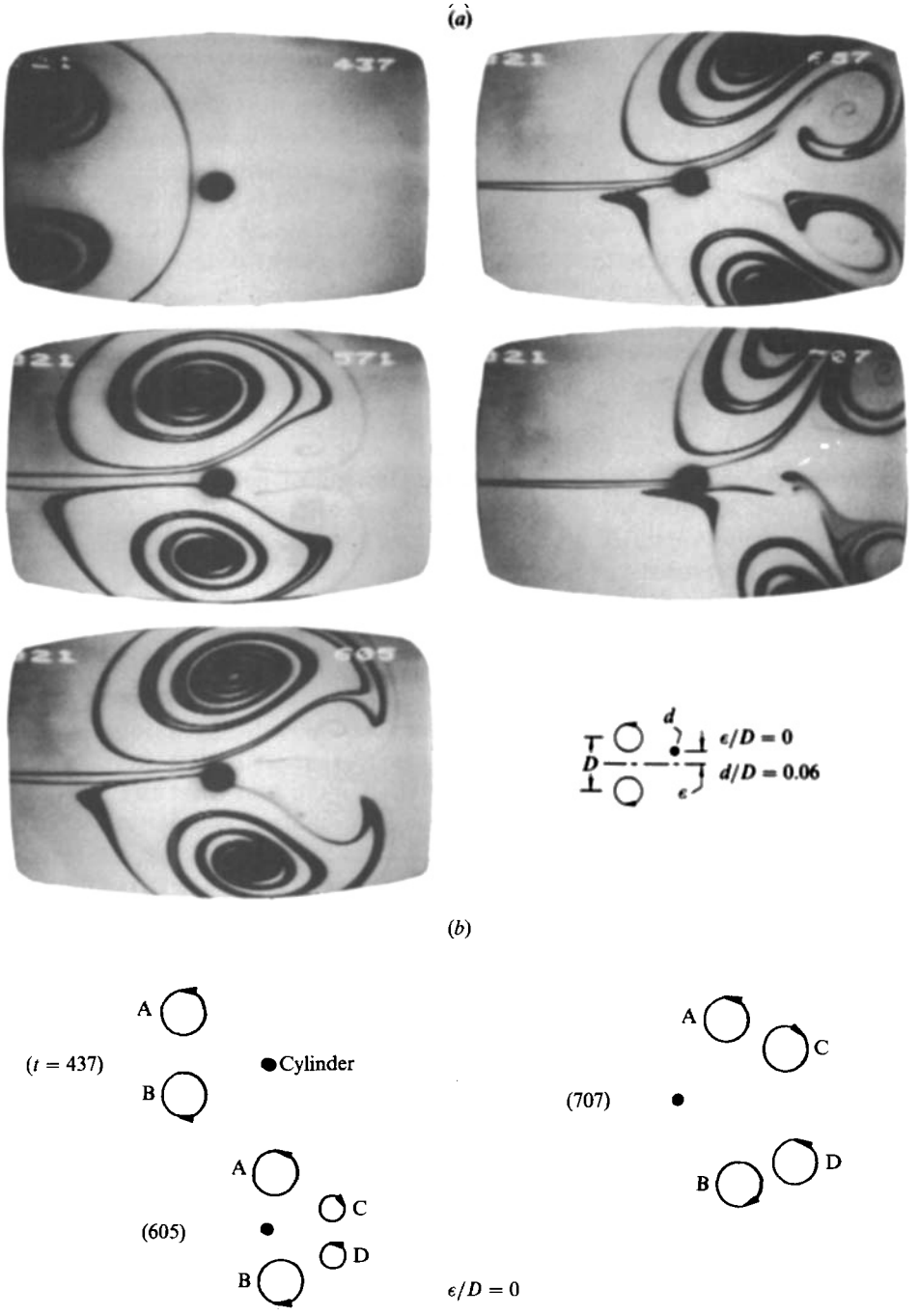

FIGURE 7. (*a*) Symmetrical mode of secondary vortex formation from small cylinder equidistant between centres of primary vortex pair; 0.06. (Actual cylinder diameter is smaller than shown in photos owing to end mount.) (*b*) Schematic representing central features of symmetrical mode of secondary vortex formation from small cylinder equidistant between centres of primary vortex pair. (Numbers in parentheses correspond to frame numbers at upper right of corresponding photos in *a*.) $\epsilon/D = 0$, $d/D = 0.06$.

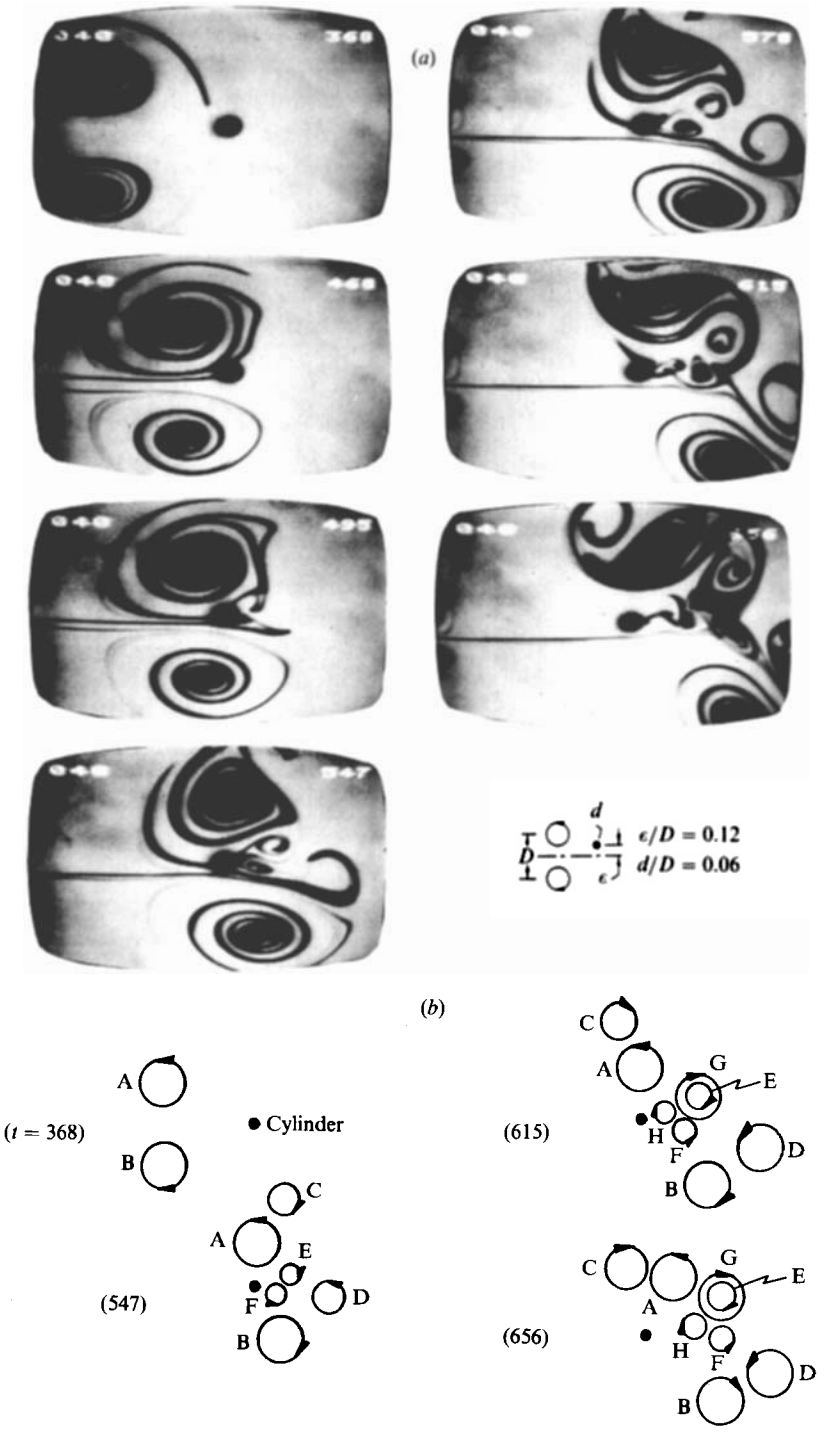

FIGURE 8. (*a*) Antisymmetrical shedding of secondary vortices from cylinder slightly displaced from centreline of primary vortex pair. (*b*) Schematic representing central features of antisymmetrical shedding of secondary vortices from cylinder slightly displaced from centreline of primary vortex. (Numbers in parentheses correspond to frame numbers at upper right of corresponding photos in *a*). $\epsilon/D = 0.12$, $d/D = 0.06$.

scale secondary vortices from the cylinder, the antisymmetrical mode of figure 8 shows small-scale antisymmetrical vortex shedding from the cylinder in the upper region and a large-scale secondary vortex in the lower region.

We first examine the structure in the lower region of figure 8. It is evident that the secondary vortex D rapidly forms as the dye marker shoots below the cylinder and rolls up in the fourth and fifth photos. In the sixth and seventh photos the vortex pair BD formed by the secondary vortex D and the corresponding primary vortex B shoots downward at an angle of approximately 45° in a fashion somewhat similar to the lower primary–secondary vortex pair of figure 7.

Concerning the flow structure in the upper region of figure 8, it is considerably more complex. The small-scale asymmetrical shedding process leads to formation of two large-scale secondary vortices C and G of like sense in addition to the incident primary vortex A. The onset of these two large-scale vortices is indicated in the third photo by the two dye indentations on the right side of the incident primary vortex. The leading vortex C on the periphery grows to relatively large scale as seen successively in photos 3–7, evident in the left-most dye rollup in the seventh photo. On the other hand, the second large-scale vortex G forming on the periphery engulfs a smaller scale vortex E shed from the cylinder, in turn forming a vortex pair AG(E) with the upper primary vortex A, evident in the fifth and sixth photos. Examination of this pattern at a later time (in the seventh photo) shows that this vortex pair AG(E) shoots upward initially at an angle of about 60°; in essence, we see that the effect on the upper primary vortex A of this complex secondary vortex shedding is to delay formation of the large-scale primary-secondary vortex pair AG(E) relative to the pair BD formed on the bottom side of the cylinder where the primary vortex B remains relatively undisturbed.

Antisymmetrical shedding of secondary vortices C and D from the cylinder located near the centre of the primary vortex A is depicted in figure 9. Subsequently, there is formation of vortex E which engulfs vortex D. At later times, there is significant interaction between the central portion of the incident primary vortex A and the cylinder. Small-scale antisymmetrical shedding from the cylinder persists as a predominant feature of this continued interaction. There is a remarkable 'peeling away' of the upper primary vortex A until, as shown in the seventh photo, the entire primary vortex appears to be converted to a complex arrangement of vorticity. As in the foregoing case, the leading secondary vortex C on the periphery of the primary vortex A forms a large-scale vortex that remains distinct.

On the other hand, the lower primary vortex B proceeds relatively undistorted. There is no formation of a corresponding secondary vortex, as in previous cases. However, there is a downward deflection of the trajectory of vortex B, apparently due to loss of circulation of the upper primary vortex (see seventh photo in figure 9).

Antisymmetrical shedding of secondary vortices from the cylinder located on the outer periphery of the primary vortex is show in figure 10. In this case, the primary vortex pair AB proceeds relatively undistorted past the cylinder. The leading secondary vortex C formed on the periphery of the primary vortex is born later than in previous cases, and does not have the opportunity to fully form; it, along with the remainder of the vortex street D and E, is eventually drawn between the primary vortices. Throughout this interaction, the central portion of the upper primary vortex remains relatively intact.

Figure 11 shows a comparison of the trajectories of the centres of the upper and lower primary vortices for the four basic interaction patterns described in the

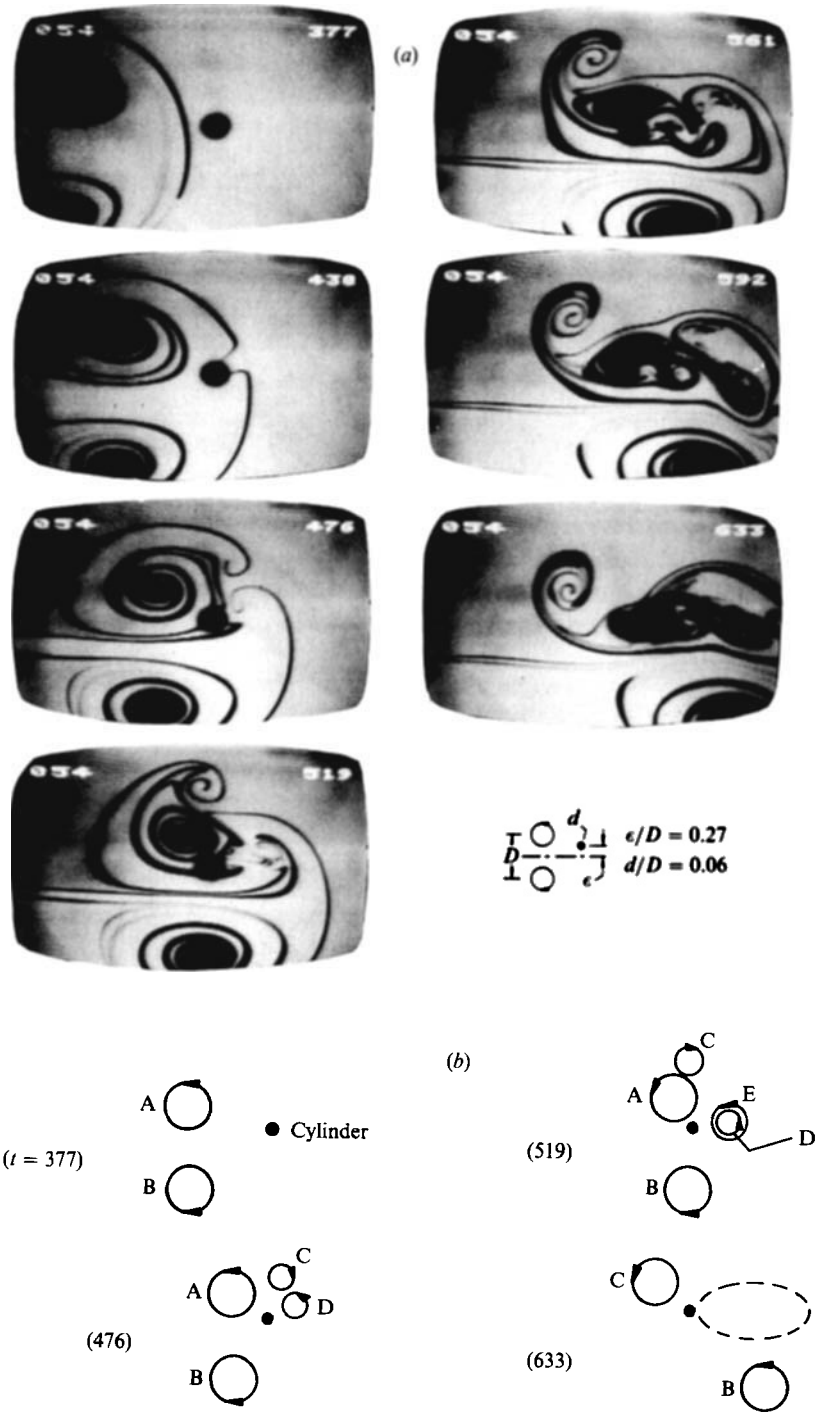

FIGURE 9. (*a*) Antisymmetrical shedding of secondary vortices from cylinder near to centre of core of primary vortex. (*b*) Schematic representing central features of antisymmetrical shedding of secondary vortices from cylinder near to centre of core of primary vortex. (Numbers in parentheses correspond to frame numbers at upper right of corresponding photos in *a*.) $\epsilon/D = 0.27, d/D = 0.06$.

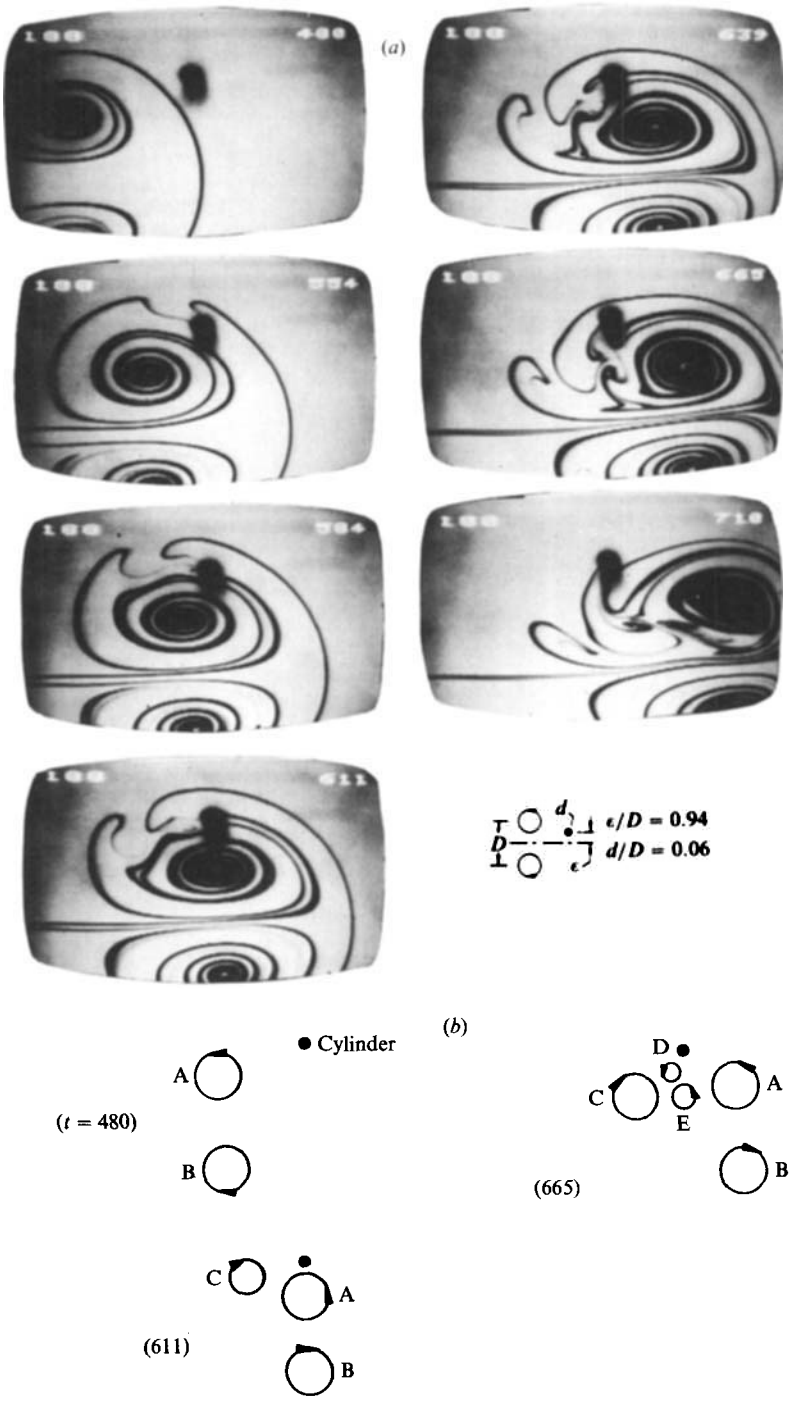

FIGURE 10. (*a*) Antisymmetrical shedding of secondary vortices from cylinder on outer periphery of primary vortex. (*b*) Schematic representing central features of antisymmetrical shedding of secondary vortices from cylinder on outer periphery of primary vortex. $\epsilon/D = 0.94$ and $d/D = 0.06$.

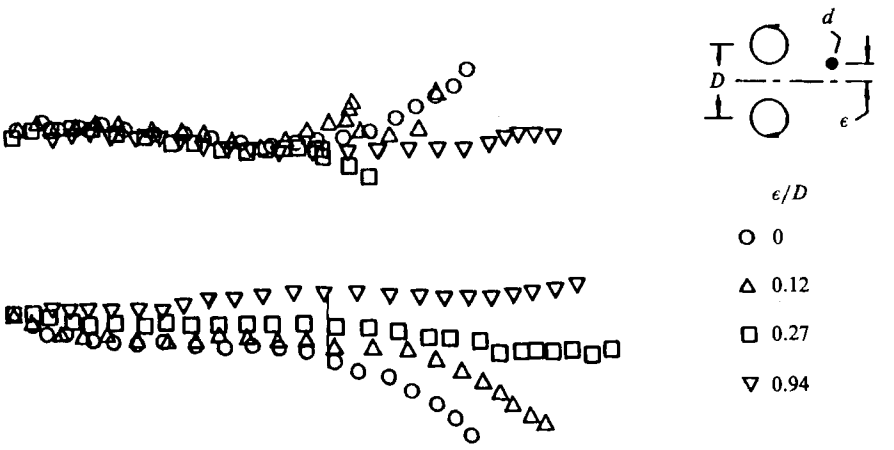

FIGURE 11. Trajectories of upper and lower primary vortices for vortex pair–cylinder interaction mechanisms corresponding to $\epsilon/D = 0$, 0.12, 0.27 and 0.94.

foregoing. In determining these trajectories, the centre of dye concentration of each primary vortex was tracked; in view of the fact that the primary vortex experiences significant distortion in some cases, such trajectories must be viewed as approximate. Nevertheless, they do provide an indiction of which types of secondary vortex generation most strongly influence the incident vortex pair. It should be noted that the time elapsed between data points in each trajectory is constant, providing an indication as to what degree the local velocity of the primary vortex changes with time and spatial position. We first address the trajectories of the lower primary vortex; for all interactions with the cylinder, the consequence of secondary vortex generation is to deflect the lower primary vortex away from the centreline of the original vortex pair. The symmetrical mode ($\epsilon/D = 0$) involving large-scale secondary vortex formation produces the most rapid distortion of the trajectories of the lower primary vortex. Concerning the trajectories of the upper primary vortices, they were traced as long as it was possible to discern the dyed vortex centre. Only when there is secondary vortex formation originating on the outer periphery of the primary vortex ($e/D = 0.94$; figure 10) does the upper primary vortex approximately maintain its horizontal trajectory.

6. The structure of the vortex–aligned plate interaction

If the small cylinder is replaced by a finite-length, thin plate (with streamlined edges) aligned with the axis of the incident vortex pair, we expect qualitatively similar generation of secondary vortices when the plate has zero offset with respect to the incident pair. However, in the case that the plate is not along the centreline of the incident vortices, the asymmetry of the secondary vortex generation, in combination with a phase delay between events at the leading and trailing edges of the plate due to its finite length, will give rise to different interaction mechanisms, relative to those described in the foregoing. As will be demonstrated, the small-scale antisymmetrical shedding prevalent in the foregoing antisymmetrical mode patterns does not occur from the trailing end of the plate; rather, the mechanisms of large-scale secondary vortex generation persist in all antisymmetrical mode interactions.

The left column of photos of figure 12 shows the symmetrical mode of secondary vortex formation from a plate located equidistant between centres of the primary

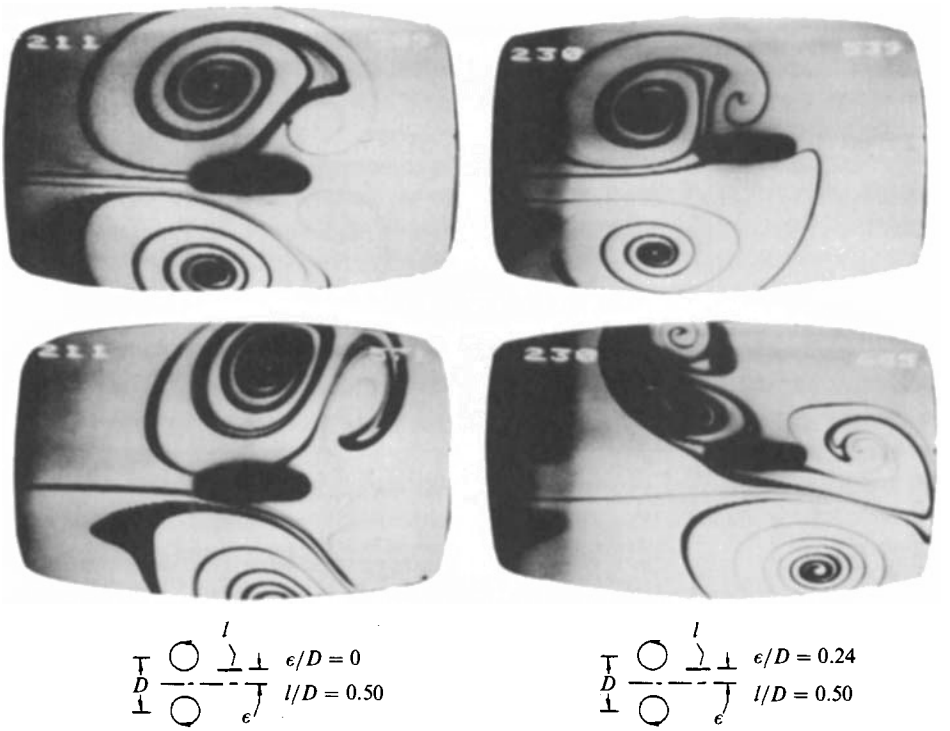

FIGURE 12. Symmetrical mode of secondary vortex formation from a plate equidistant between centres of primary vortex pair; $\epsilon/D = 0$, $l/D = 0.50$ (left column of photos); and antisymmetrical mode of secondary vortex formation from plate located between axis of incident (primary) vortex pair and centre of primary vortex; $\epsilon/D = 0.24$, $l/D = 0.50$ (right column of photos). (Thickness of plate $t/D = 0.06$ is smaller than shown in photos owing to end mount.)

vortex pair. In the upper photo, the separated shear layers have evolved to a pronounced secondary vortex pair. By the time the centres of the incident primary vortices have reached the centre of the plate (see bottom photo), the accompanying secondary vortices are well developed. The newly formed primary–secondary pairs travel off at an angle of about 60°.

Comparing a large number of photos (not shown here) in the time series corresponding to the symmetrical interaction in the left column of figure 12 with the corresponding one of figure 7 for the cylinder interaction, one sees a remarkable similarity in not only the basic features of the primary–secondary vortex patterns, but also in the rate of growth of the secondary vortices. Keeping in mind that the cylinder has a much smaller lengthscale than the plate, i.e. $d/D = 0.06$ as compared with $d/D = 0.50$, it is possible to conclude that once separation of the wall viscous layer is induced by the arrival of the primary vortex, the growth of the secondary instability is relatively independent of the body lengthscale; only the trajectory of the primary–secondary vortex pair is significantly influenced.

If the plate is moved away from the centre of the upper primary vortex, there is rapid formation of a secondary vortex from the upper surface of the plate, as indicated in the right column of photos of figure 12. The consequent primary–secondary vortex pair in the upper region of the flow moves upstream at a small angle with respect to the axis of the plate. Correspondingly, the vortex pair from the lower side of the plate departs at a small angle as well.

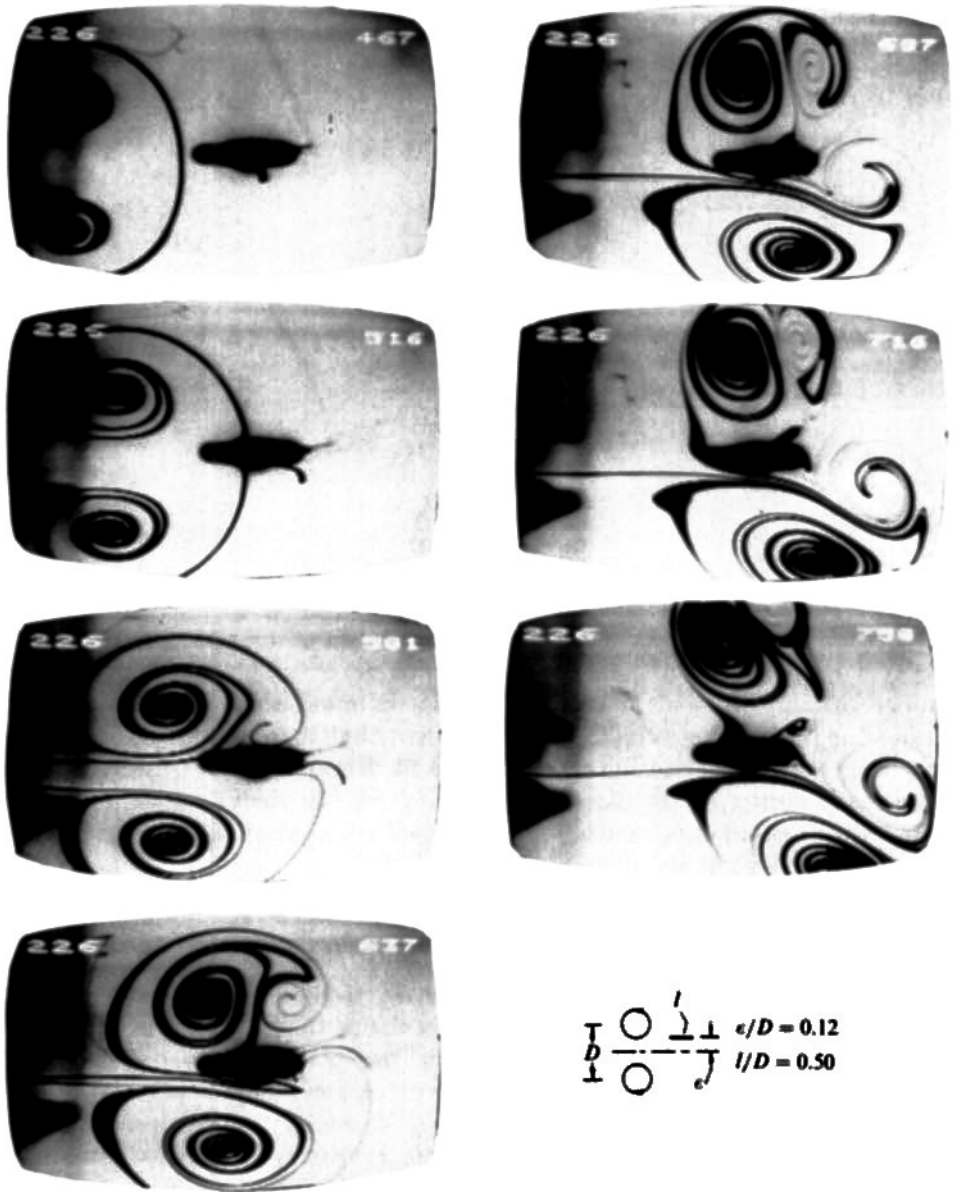

FIGURE 13. Antisymmetrical mode of secondary vortex formation from plate slightly displaced from centreline of incident vortex pair; $\epsilon/D = 0.12$, $l/D = 0.50$.

Figure 13 compares a complete sequence of the encounter of the vortex pair with a plate offset a distance $\epsilon/D = 0.12$, a value between the two extremes of figure 12. In a similar fashion as for the series at the bottom of figure 12, the end consequence is a system of the vortex pairs, one moving upstream and the other downstream, of somewhat large angles with respect to the axis of the plate.

Figure 14 shows trajectories of the centres of the primary vortices for the three interaction patterns described in the foregoing. The lower family of trajectories, corresponding to the path of the lower primary vortex, shows that there is earlier deflection away from the centreline when the plate is moved towards the centre of

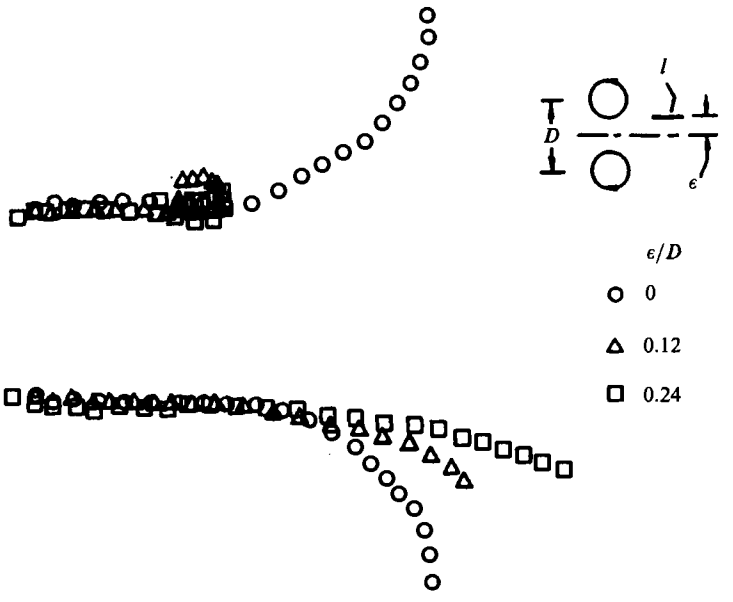

FIGURE 14. Trajectories of primary vortices corresponding to vortex–aligned plate interactions for offsets $\epsilon/D = 0$, 0.12 and 0.24.

the upper primary vortex. Moreover, keeping in mind that data points have a constant time interval between them, it is evident that there is eventual retardation of the primary vortex speed for $\epsilon/D = 0.12$, 0.24. Regarding the trajectories of the upper primary vortex, as the plate is moved towards the vortex centre ($\epsilon/D = 0.12$, 0.34), it induces rapid deceleration, and eventual reversal of the vortex trajectory near the leading edge of the plate.

7. The structure of the vortex–orthogonal plate interaction

In the event that a plate is oriented orthogonally to the incident vortex pair, then there results the types of interactions shown in figure 15. In the top row of photos, collision of the upper primary vortex with the plate terminates its forward translation: there is formation of a secondary vortex due to flow separation from the surface of the plate, and the resultant primary–secondary vortex pair eventually moves in the upstream direction. The lower primary vortex is deflected downwards; the secondary vortex formed from the surface of the plate joins with its primary vortex counterpart to form a translating vortex pair.

For the series represented in the middle row of photos of figure 14, the upper primary vortex is detained; formation of the secondary vortex from the corner of the plate eventually draws the dye marker originally representing the upper primary vortex past the corner of the plate and into the region between the secondary vortex and the lower primary vortex.

In the bottom row of photos, there is simply distortion of the upper primary vortex as it encounters the lower edge of the plate. The integrity of the central portion of its core is apparently retained, and the long 'tail' of the outer portion of the vortex is drawn into the region between the two primary vortices.

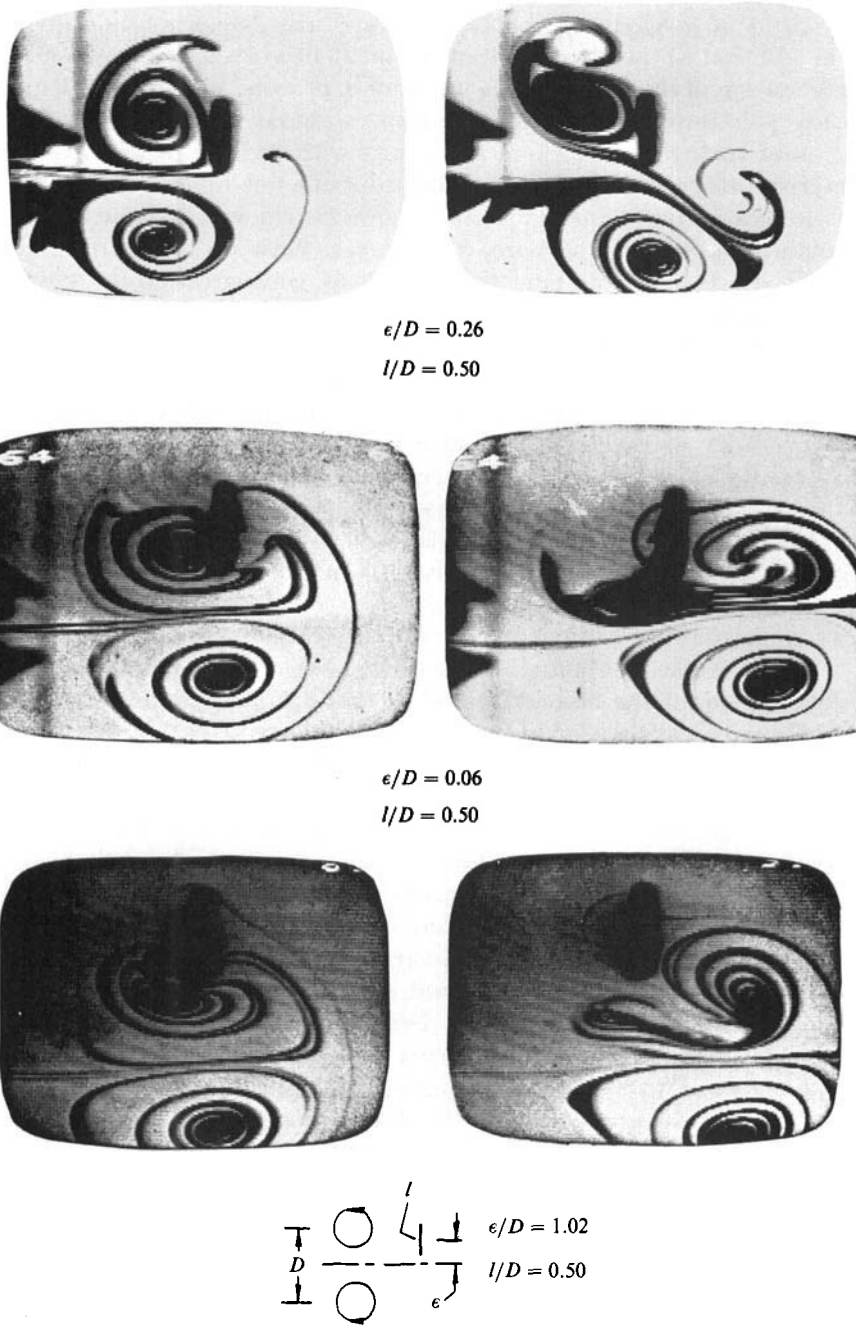

FIGURE 15. Types of interaction of incident vortex pair with orthogonally oriented plate; $\epsilon/D = 0.26, 0.06, 1.02$; $l/D = 0.50$.

8. Concluding remarks

When a vortex is incident upon a solid surface, the degree of concentration of vorticity, in addition to the circulation of the incident vortex(ices) is essential for a full characterization of the details of the interaction process. Vorticity measurements of the vortex pair impulsively generated from a planar nozzle show a degree of concentration of vorticity in excellent agreement with inviscid theory, even though the characteristic Reynolds number is of the order of a few hundred. This adequacy of the inviscid description is analogous to the success achieved in describing neutral, nonlinear disturbances in periodic free shear layers between two uniform streams (Stuart 1967). In this simulation, the degree of concentration of vorticity is arbitrary, and agrees well with an experimentally generated case at low Reynolds number (Ziada & Rockwell 1982).

To examine the basic characteristics of large-scale secondary formation, we have considered the case of vortex pairs symmetrically incident upon a body having a lengthscale an order of magnitude smaller than the incident vortex pair (small cylinder). Vorticity measurements were carried out at a representative cross-section downstream of the body; this section was located at a streamwise distance downstream of the body within the lengthscale of the incident vortex pair, yet sufficiently far downstream of the body that the initial stage of secondary vortex formation was attained. The relative circulation of the primary and secondary vortices was approximated from these vorticity measurements. The secondary vortex reaches a circulation approximately equal to that of the primary vortex at a distance downstream of the body of less than half the lengthscale of the incident vortex pair. Moreover, evaluation of the integral of the vorticity (squared) across the flow for the primary and secondary vortices provides insight into the basis for the formation of a primary–secondary vortex pair whereby the centres of the primary and secondary vortices move at the same convective speed. In fact, formation of such primary–secondary vortex pairs was found to be a central element of all of the interaction patterns for which there was generation of a large-scale secondary vortex. Moreover, the occurrence of the maximum in the vorticity was preceded by its exponential amplification for both the primary and the secondary vortices.

In this investigation, we have considered interaction of the incident (primary) vortex pair with bodies of various scales. Defining the lengthscale of the incident vortex pair as the distance between the vortex centres, the lengthscales of the bodies range from the order of, to two orders of magnitude smaller than, that of the incident vortex pair. Central to nearly all of the interaction patterns is generation of secondary vortices of opposite sense relative to those of the corresponding primary (incident) vortices; these large-scale secondary vortices arise from separation of the viscous layer on the surface of the body, followed by rapid growth of the perturbed layer. The basic modal structures of secondary vortex generation depend upon the degree of symmetry of the primary vortex–body encounter and, in some cases, on the lengthscale of the body. In the symmetrical mode of secondary vortex generation, arising from a vortex pair symmetrically incident upon the centreline of the body, there is always rapid, in-phase formation of large-scale secondary vortices, irrespective of the lengthscale of the body relative to that of the incident vortex pair. On the other hand, secondary vortex formation in the antisymmetrical mode, arising from initial asymmetry of the vortex-pair–body interaction, can take on two basic forms: a small-scale antisymmetrical vortex street having the same scale as the body width; or, large-scale secondary vortices that are generated with a phase difference

between them due to the finite lengthscale of the body. The former type of antisymmetrical mode occurs for cases where the body has lengthscale about an order of magnitude smaller than that of the incident vortex pair, while the latter antisymmetrical mode occurs for body length-scales of the order of the incident pair. Moreover, in all cases where a large-scale secondary vortex is generated during the interaction process, it tends to form a counter-rotating vortex pair with its corresponding primary vortex, in turn influencing the trajectory of the primary vortex.

For the case where the lengthscale of the body is at least an order of magnitude smaller than the scale of the incident vortex pair, the interaction pattern changes abruptly in going from the symmetrical to antisymmetrical mode of secondary vortex formation. Whereas the symmetrical mode produces large-scale secondary vortices that abruptly alter the trajectories of the corresponding primary vortices, the antisymmetrical mode, involving generation of a small-scale antisymmetrical vortex street (secondary vortices), has a relatively local effect, primarily altering the core structure of the primary vortex. Several types of patterns occur, the most interesting being a gradual 'peeling away' of the core of the primary vortex, whereby it is transformed into the vortex street of the cylinder. In such cases, the structure and trajectory of the unaffected (neighbouring) primary vortex are relatively undistorted, at least in the very near field.

In the event that the body (plate) has a streamwise lengthscale of the same order as that of the vortex pair and is in-line with the centreplane of the incident vortex pair, the type of large-scale (secondary) vortex formation is very similar to that generated from small bodies. However, if the incident vortex encounter is not symmetrical, then secondary vortex shedding does not occur from the trailing end of the plate as in the case of small bodies; rather, there is formation of large-scale secondary vortices from the surface of the plate upstream of the trailing end, with the time lag (phase shift) between their formation related to the length of the plate. In fact, the magnitude of the phase shift is determined by the distances between separation locations on the plate that lead to formation of two secondary vortices.

This research program was funded by the Office of Naval Research and the National Science Foundation.

REFERENCES

BATCHELOR, G. K. 1967 *An Introduction to Fluid Dynamics*. Cambridge University Press.

BUSHNELL, D. M. 1984 Body–turbulence interaction. *AIAA Paper* 84–1527. Presented at *17th Fluid Dynamics, Plasma Dynamics, and Lasers Conference, June 25, 1984, Snowmass, Colorado.*

CERRA, A. & SMITH, C. 1983 Experimental observations of vortex ring interaction with the fluid adjacent to the surface. *Rep* Fm-4, Lehigh University, AFOSR Tr-84-0130, 80A, No. 138999, 178 pp.

DIDDEN, N. & HO, C.-M. 1985 Unsteady separation in a boundary layer produced by an impinging jet. *J. Fluid Mech.* **160**, 235–256.

DOLIGALSKI, T. L., SMITH, C. R. & WALKER, J. D. A. 1979 Production mechanism for turbulent boundary-layer flows. *Symp. on Viscous Drag Reduction, Dallas, Texas, November 7–8.*

DOLIGALSKI, T. L. & WALKER, J. D. A. 1984 Boundary layer induced by a convected two-dimensional vortex. *J. Fluid Mech.*, **139**, 1–28.

HARVEY, J. K. & PERRY, F. J. 1971 Flow field produced by trailing vortices in the vicinity of the ground. *AIAA J.*, **9**, 1569–1616.

Ho, C.-M. 1983 An alternative look at the unsteady separation phenomenon. In *Recent Advances in Aerodynamics, Proc. Int. Symp., Stanford University, August 22–26*, pp. 165–178, Springer.

Homa, J. 1984 Interactions of an impulsively-generated two-dimensional vortex pair with flat plates and cylinders. M.S. thesis, Department of Mechanical Engineering and Mechanics, Lehigh University, Bethlehem, Pa.

Homa, J. & Rockwell, D. 1983 Vortex–body interaction. *Bull. Am. Phys. Soc.* **28**, 1365.

Kaykayoglu, R. & Rockwell, D. 1985 Vortices incident upon a leading-edge: instantaneous pressure fields. *J. Fluid Mech.*, **156**, 439–461.

Kaykayoglu, R. & Rockwell, D. 1986 Unstable jet–edge interaction. Part 1. Instantaneous pressure fields at a single frequency. *J. Fluid Mech.*, **169**, 125–149.

Kiya, M., Ohyama, M. & Hunt, J. C. R. 1986 Vortex pairs and rings interacting with shear layer vortices. *J. Fluid Mech.* **172**, 1–17.

Lamb, H. 1932 *Hydrodynamics*, 6th edn. p. 223. Dover.

Magarvey, R. H. & MacLatchy, C. S. 1964 The disintegration of vortex rings. *Can. J. Phys.* **42**, 684–689.

Panaras, A. G. 1985 Pressure pulses generated by the interaction of a discrete vortex with an edge. *J. Fluid Mech.* **154**, 445–462.

Panaras, A. G. 1986 Simulation of impinging shear layers using vortex dynamics. *AGARD/FDP, Round Table Discussion Aix-en-Provence, 10 April.*

Panaras, A. G. 1987 Numerical modelling of the vortex–airfoil interaction. *AIAA J.* **25**, 5–11.

Rockwell, D. 1983 Invited lecture: Oscillations of impinging shear layers. *AIAA J.* **21**, 645–664.

Rockwell, D. 1984 Unsteady loading of leading-edges in unstable flows – an overview. *AIAA Paper* 84-2306

Schneider, P. E. M. 1978 Morphologisch-phaenomenologische Unterschung der Umbildung von Ringwirbeln, die Koerper anstroemen. *Rep.* 14–1978, Max-Planck-Institut fuer Stroemungsforschung, Goettingen, West Germany.

Schneider, P. E. M. 1980 Sekundaerwirbelbildung bei Ringwirbeln und in Freistrahlen. *Z. Flugwiss. Weltraumforsch.* **4**, 307–317.

Stuart, J. T. 1967 On finite amplitude oscillations in laminar mixing layers. *J. Fluid Mech.* **29**, 417–440.

Sullivan, J. P., Widnall, S. E. & Ezekiel, S. 1973 Study of vortex rings using a Laser-Doppler velocimeter. *AIAA J.* **11**, 1384–1389.

Walker, J. D. A. 1978 The boundary layer due to rectilinear vortex. *Proc. R. Soc. Lond.* A**350**, 167–188.

Ziada, S. & Rockwell, D. 1982 Vortex–leading-edge interaction. *J. Fluid Mech.* **118**, 79–107.